Chinese Chemical Letters 36 (2025) 110445

Contents lists available at ScienceDirect

Chinese Chemical Letters

journal homepage: www.elsevier.com/locate/cclet

2D hexagonal tessellations sustained by Br···Br/H contacts: From regular to semiregular to *k*-uniform tilings

Junjie Duan[a,b], Dan Chen[d], Long Chen[e], Shuying Li[c,*], Ting Chen[a,*], Dong Wang[a,b]

[a] CAS Key Laboratory of Molecular Nanostructure and Nanotechnology, CAS Research/Education Center for Excellence in Molecular Sciences, Beijing National Laboratory for Molecular Sciences (BNLMS), Institute of Chemistry, Chinese Academy of Sciences, Beijing 100190, China
[b] University of Chinese Academy of Sciences, Beijing 100049, China
[c] Department of Chemistry, Northeast Normal University, Changchun 130024, China
[d] Instrumental Analysis Center, Shanghai Jiao Tong University, Shanghai 200240, China
[e] State Key Laboratory of Supramolecular Structure and Mate-rials, College of Chemistry, Jilin University, Changchun 130012, China

ARTICLE INFO

Article history:
Received 1 May 2024
Revised 9 September 2024
Accepted 10 September 2024
Available online 11 September 2024

Keywords:
2D tessellation
Molecular self-assembly
Scanning tunneling microscopy
Noncovalent interactions

ABSTRACT

Achieving seamless tiling through the self-assembly of organic species has long fascinated scientists for its potential applications across various fields. However, constructing periodic nanostructures with high-order tessellation remains challenging, particularly in achieving precise control at the supramolecular level. In this study, we present the successful creation of multiple seamless 2D tessellations on Au (111) surface using versatile hexagonal tiles derived from a singular molecular unit, namely 2,6,10-tribromotricycloquinazoline. Through scanning tunneling microscopy imaging, seven distinct 2D tessellations, ranging from regular to semiregular to *k*-uniform tilings, are unveiled at the molecular level. Density functional theory calculations provide a theoretical basis for the formation of these complex 2D tessellation, highlighting the important role of the variability of Br···Br/H contacts in facilitating complex seamless 2D tessellations on surface. This work opens avenues for exploring possibilities in constructing intricate tiling patterns with diverse applications.

Two-dimensional (2D) tessellation by regular polygons is a fundamental concept with potential applications in mathematics, chemistry, physics, and biology [1-5]. Many natural phenomena and organisms, such as beehives and coral structures, exhibit intricate and ordered 2D patterns. In-depth research into 2D tessellation provides insights from nature, helping understand how these organisms organize and optimize space, thus advancing fields like nanotechnology and materials science. Construction principles of 2D tessellation have been extensively studied and represented in numerous regular or semiregular phases [6-8]. One typical 2D tessellation is Archimedean tiling (AT), which consists of one or more types of polygonal constitutes filling the entire plane in an edge-to-edge manner without gaps, with all the vertices in the tessellation belonging to the same type. Eleven distinct 2D AT patterns have been proposed in the past, three of which are regular tiling, composed of only one type of polygon, such as triangles, squares, and hexagons [9]. The remaining eight ATs involve a variety of different polygons, which are called semi-regular tiling [10-12]. When the condition of the vertex type is relaxed to multiple types of vertices, the tessellation is called *k*-uniform tiling, where *k* is the number of distinct types of vertices [13]. Notably, constructing periodic nanostructures with higher-order tessellation remains challenging, particularly in achieving precise control at the supramolecular level.

By controlling the assembly behavior of molecules at the molecular level, interfacial supramolecular chemistry offers innovative approaches to developing new materials and addressing issues in biomedical, environmental, and energy-related areas. Recent progress in interfacial supramolecular chemistry provides fascinating bottom-up approach to fabricate 2D ATs and other complex tessellations on surfaces [14-18]. Utilizing the interplay between adjacent functional groups within molecules and the interactions between molecules and substrates, a diverse array of 2D tessellation patterns have been constructed and characterized through the application of scanning tunneling microscopy (STM) [19-21]. For instance, using a single dissymmetric precursor, long-range ordered semi-regular (3.4.6.4) AT on an atomically flat Ag(111) surface has been achieved through a multi-step interfacial chemical reaction [22]. Peter H. Beton and co-workers reported a set of random tiling networks in which the degree of randomness varies with small changes in the chemical en-

* Corresponding authors.
E-mail addresses: lisy878@nenu.edu.cn (S. Li), chenting@iccas.ac.cn (T. Chen).

https://doi.org/10.1016/j.cclet.2024.110445
1001-8417/

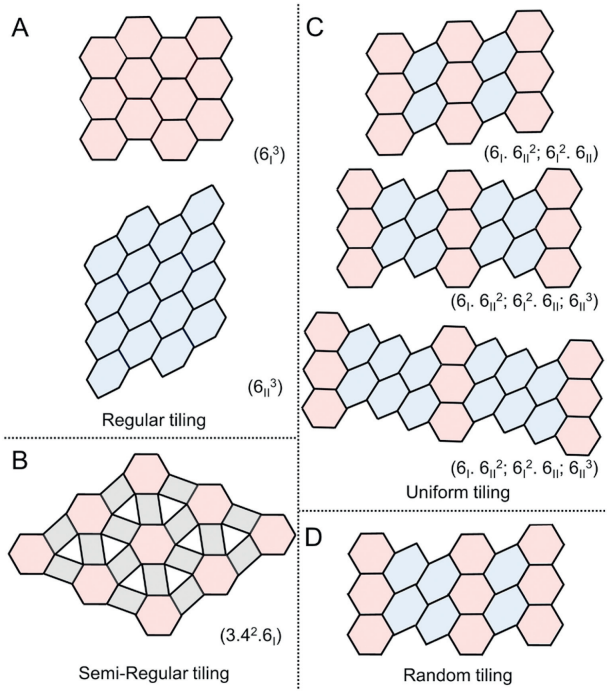

Scheme 1. Illustration of diverse 2D tessellations formed by TBTCQ on Au (111). (A) Regular tiling with only one type of vertex. (B) Semi-regular tiling with only one type of vertex but more than one types of polygons at each vertex. (C) Uniform tiling with two or three types of vertices. (D) Random tiling.

vironment in the system [23]. As a non-covalent force, halogen bonding plays a pivotal role in the construction of 2D nanostructures [16,24,25]. It facilitates the establishment of stable connections between diverse molecules, while the directional and selective nature of halogen bonding guides the oriented arrangement of molecules. These unique interaction properties endow it exceptional building capabilities, offering abundant possibilities for the design and application of supramolecular structures. However, the complex tiling without gaps and overlaps based on flexible building blocks directed by non-covalent halogen-bond remains largely unexplored. Herein, we present a diverse range of 2D seamless tessellations based on a singular building block, 2,6,10-tribromotricycloquinazoline (TBTCQ), adsorbed on a Au (111) surface. STM imaging indicate that the TBTCQ molecules participate in the formation of 2D tessellation primarily in two different arrangements through Br···Br/H contacts, resulting in five hexagonal tiles. But only two of them can form regular or one semi-regular 2D tilings on Au (111). Further interweaving of these two hexagonal tiles gives rise to three more complex *k*-uniform tiling and one random tiling motifs (Scheme 1). It is suggested that the emergence of manifold tessellations in the self-assembly of TBTCQ originates from the flexible Br···Br/H contacts formed between adjacent molecular building blocks. Our results introduce a novel strategy for fabricating complex 2D tessellation, utilizing the flexibility of halogen-mediated interactions.

The molecular structure and the electrostatic potential map of TBTCQ is depicted in Fig. 1A, revealing distinct positive σ-holes and negatively charged regions along the equator on the bromine atoms. Despite being achiral, TBTCQ molecule can form two enantiomeric adsorption conformations, *r*-TBTCQ and *s*-TBTCQ, on the surface due to the restriction of off-plane flipping (Fig. S2A in Supporting information). Upon deposition on Au (111), STM imaging shows TBTCQ molecules appearing as a ternary windmill configuration. According to the inclined direction of the windmill blades, two mirror-imaged enantiomers are resolved in the STM images. They separate spontaneously and form homochiral domains constituted of enantiopure *r*-TBTCQ or *s*-TBTCQ (Figs. S2B and C in Supporting information). For clarity, the 2D tiling of *r*-TBTCQ is discussed for example in the following.

Careful inspection of the STM images allow us to identify two elementary structural units (Type I dimer and Type II dimer) that underlie the supramolecular motifs. The corresponding molecular models of the dimer units are displayed in Fig. 1B. The relative positions of the two molecules within Type I and Type II dimers are different. Specifically, the molecule on the left lies higher than the molecule on the right in Type I dimer, whereas it is just the opposite in Type II dimer. However, both Type I and Type II dimers are stabilized by interactions mediated by the Br atoms, including Br···Br and Br···H interactions. Based on the two dimer units, five hexagonal tiles are fabricated on the surface (Fig. S3 in Supporting information and Figs. 1C-G), which are named Hex-I, Hex-II, Hex-III, Hex-IV, and Hex-V, respectively. Hex-I (Hex-V) is composed exclusively of six Type I (Type II) dimers. However, Hex-II, III, and IV contain both Type I and Type II dimers. From Hex-III to Hex-IV, the number of Type I dimer decreases from 4 to 2 gradually, and the number of Type II dimer increases from 2 to 4 accordingly. Moreover, *s*-TBTCQ molecules can form the same hexagonal tiles as well (Fig. S4 in Supporting information).

Only Hex-I and Hex-II can form regular 2D tilings on Au (111). The 2D tiling based on Hex-I exhibits two distinct structures (Fig. S5 in Supporting information). In Phase I (Fig. 2A), Hex-I tiles meet at each side of the hexagon, and molecular centers are positioned at the vertices of the hexagonal unit. The unit cell parameters of Phase I are measured to be $a = b = 2.1 \pm 0.1$ nm, $\theta = 60° \pm 1°$. The unit cell of Phase I exhibits an offset of $20° \pm 1°$ with respect to the ⟨110⟩ direction of the substrate. The other tessellation Phase II of Hex-I can be seen as a derivative of Phase I, in which the distance between Hex-I tiles is enlarged (Fig. 2B). The adjacent Hex-I tiles are stabilized by a X_4-type Br···Br interactions [26]. A unit cell is superimposed in the STM motif of Phase II, in which $a = b = 3.6 \pm 0.1$ nm and $\theta = 60° \pm 1°$. The unit cell of Phase II exhibits an offset of $20° \pm 1°$ with respect to the ⟨110⟩ direction of the substrate as well. The 2D tiling can be described using a series of integers ($n_1{}^{\alpha_1}$. $n_2{}^{\alpha_2}$.... $n_n{}^{\alpha_n}$), in which each integer reflects the number of sides n_i of the polygons converging at a given vertex [27]. The order of the polygons is denoted in a clockwise manner, and if there are multiple identical neighboring polygons, their quantity is indicated by the exponent α_i. As there are two distinct hexagonal tiles, *i.e.*, Hex-I and Hex-II, are involved in the 2D tiling presented here, we distinguish them as 6_I and 6_{II}, respectively. The 2D tiling in Phase I is named ($6_I{}^3$), and the 2D tiling in Phase II is expressed as a tiling ($3.4^2.6_I$). Phase II is referred as a semi-regular tiling since the structure contains more than one types of polygons at each vertex.

Besides the above two tessellations based on regular hexagonal tiles Hex-I, there is another long-range ordered tessellation (Phase III), which is composed solely of Hex-II, as displayed in Fig. 2C. The lattice parameters for Phase III are $a = 2.1 \pm 0.1$ nm, $b = 2.4 \pm 0.1$ nm, and $\theta = 48° \pm 1°$ The unit cell of Phase III exhibits an offset of $17° \pm 1°$ with respect to the ⟨110⟩ direction of the substrate. It is an irregular hexagonal lattice, which is different from Phase I and II with a regular hexagonal lattice. This is because Hex-II is made up of both type I and Type II dimers. Due to the varying distances between molecular centers in the two dimers, Hex-II tiles exhibit two kinds of edge lengths, thereby giving rise to a deformed hexagonal shape. According to the naming convention mentioned above, Phase III can be described as ($6_{II}{}^3$). Furthermore, Phase III usually coexist with multiple higher-order 2D tessellations that formed by interweaving of Hex-I and Hex-II (Fig. S6 in Supporting information).

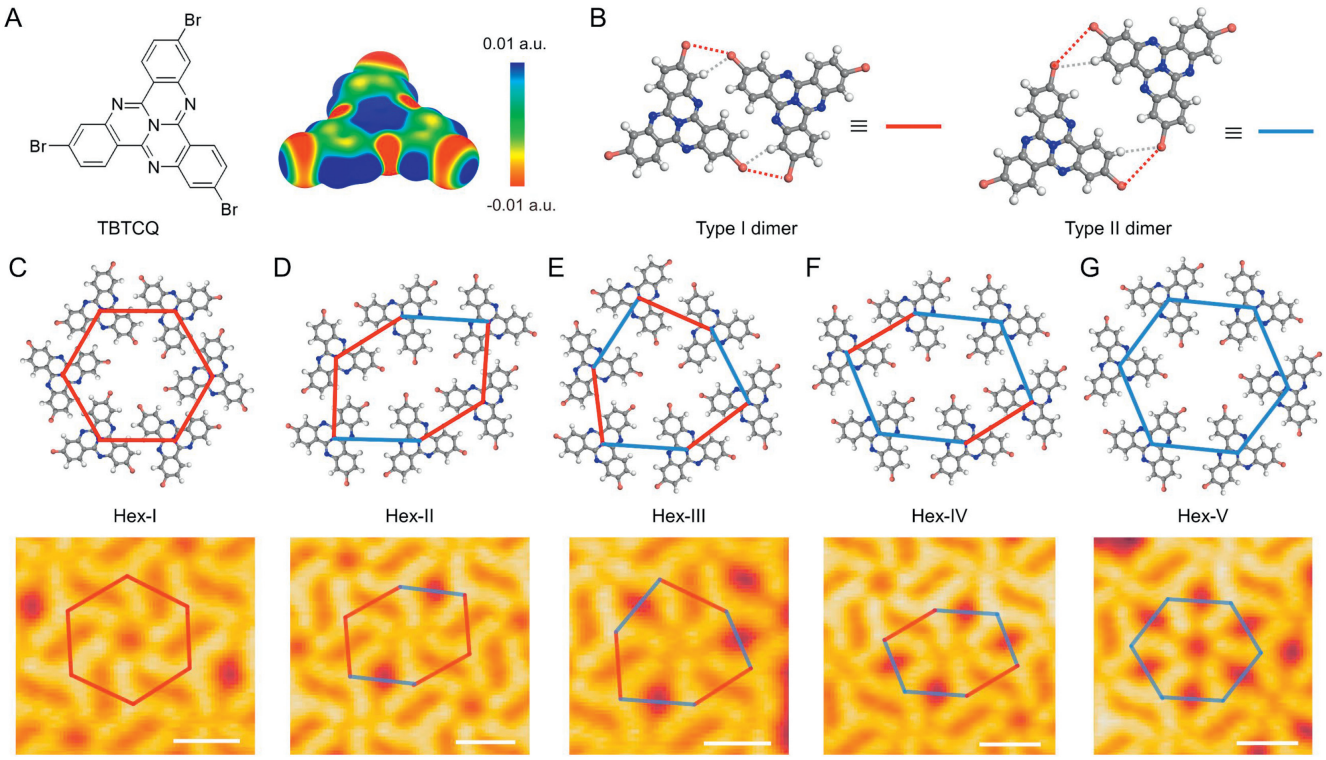

Fig. 1. Chemical structure of TBTCQ and hexagonal tiles formed based on it. (A) Molecular structure and calculated electrostatic potential map of TBTCQ. The isosurface value of the electron density is 0.001 a.u. (B) Molecular models for Type I and Type II dimers identified on Au (111) surface. For clarity, Type I and Type II dimers are denoted by a red solid line and a blue solid line, respectively. The red and gray dashed lines identify the Br···Br and Br···H interactions, respectively. (C-G) Molecular models for the hexagonal tiles formed by enantiopure *r*-TBTCQ and the corresponding STM motifs. Imaging parameters: $V_b = 310$ mV, $I_t = 300$ pA. All scale bars are 1 nm.

Fig. 3A displays the STM image for Phase IV where the composition ratio of Hex-I to Hex-II is 1:1. To be specific, Phase IV consists of alternating Hex-I columns and Hex-II columns. Therefore, it contains two types of vertices (marked with black circles), with one type encircled by one Hex-I and two Hex-II, and the other encircled by two Hex-I and one Hex-II. It is a 2-uniform tiling and labeled as (6_I. 6_{II}^2; 6_I^2. 6_{II}). As for the 2D tiling in Phase V, the molecular columns of Hex-I are uniformly separated by two columns of Hex-II (Fig. 3B). Therefore, the composition ratio of Hex-I to Hex-II in Phase V is 1:2. Except for the two types of vertices observed in Phase IV, another vertex that encircled by three Hex-II tiles are contained in Phase V (outlined by black circles). Therefore, the tessellation is a 3-uniform tiling and described as (6_I. 6_{II}^2; 6_I^2. 6_{II}; 6_{II}^3). Additionally, the number of the columns of Hex-II inserted into the Hex-I rows can further increase to three, generating long-range ordered 2D tessellation (Phase VI), as shown in the Fig. 3C. The composition ratio of Hex-I to Hex-II in Phase VI is 1:3. There are still three types of vertices in the 2D tiling in this situation. And thus, Phase VI also can be named as (6_I. 6_{II}^2; 6_I^2. 6_{II}; 6_{II}^3). Besides the regular Phase IV to VI, interweaving of Hex-I and Hex-II may give irregular 2D tessellations as well, as shown in Fig. 3D. The number of Hex-II columns inserted between two neighboring Hex-I columns is flexible in the range of one to three, giving rise to a 2D random tiling (Phase VII).

Our experimental observations indicate that Hex-I and Hex-II form seven distinct 2D tessellations on Au (111), ranging from regular to semiregular to complex *k*-uniform tiling. Additionally, Phase I can be formed under all studied molecular coverages. Phase II is preferred at low and moderate molecular coverages (lower than 0.5 ML), while Phase III composed of Hex-II as well as Phase IV-VII composed of Hex-II and Hex-II are preferred at high molecular coverage. Except for Phase II, the other 2D tessellations can coexist on the surface (Fig. S7 in Supporting information). In contrast, Hex-III, Hex-IV, and Hex-V can only be observed at the domain boundaries and do not contribute to 2D tessellation (Fig. S3). Although the model diagrams initially suggested that the regular hexagonal Hex-V could seamlessly form a tiling, and the irregular Hex-IV could either tessellate independently or co-tessellate with Hex-I or Hex-V to generate 2D tilings, this expectation does not align with our experimental findings. This discrepancy is likely related to variations in intermolecular interactions between Type I and Type II dimers. The experimental findings emphasize the prevalence of Hex-I and Hex-II in forming 2D tessellations, implying stronger intermolecular interactions in Type I dimers.

To provide a theoretical basis for the experimental results, density functional theory (DFT) calculations were conducted to estimate the adsorption energies of Type I and Type II dimers on the Au (111) surface. Initially, we examined the adsorption of an individual molecule, specifically *r*-TBTCQ, on the Au (111) surface. For the DFT simulations, we utilized the molecular orientation derived from STM experiments, indicating an angle of 25° between the line connecting Br atom and N atom in the molecular center of *r*-TBTCQ and the ⟨110⟩ direction of the substrate. Subsequently, we calculated the energies of the *r*-TBTCQ/Au (111) systems with the molecule positioned at the hole, bridge and top positions on the Au (111) surface. The results indicate that only the *r*-TBTCQ molecule adsorbed at the hole site maintained an orientation of −25° with the lowest energy, suggesting the optimal adsorption configuration for *r*-TBTCQ is centered at the hole position with a −25° orientation. Building upon this optimized configuration, we developed initial models based on the experimental data to optimize the adsorption configurations of Type I and Type II dimers. The findings revealed that the energy of the Type I dimer is lower than that of the Type II dimer by 0.07 eV, indicating greater sta-

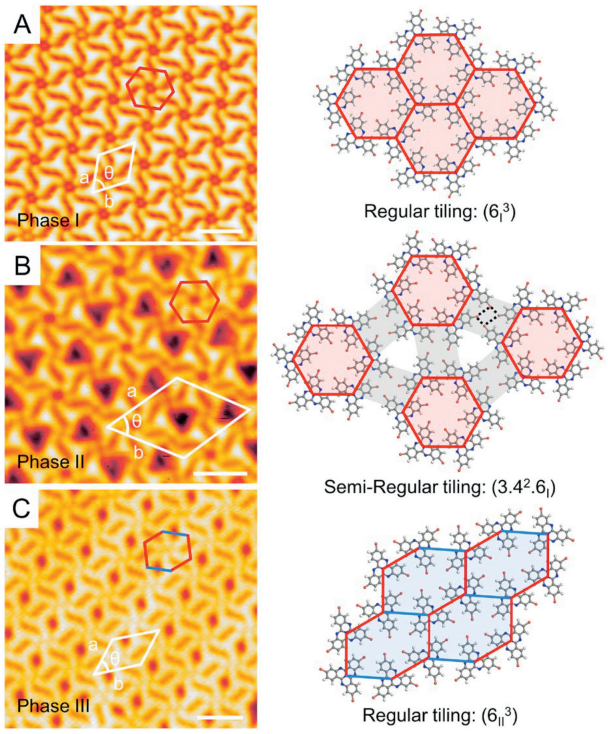

Fig. 2. 2D tessellations formed solely by Hex-I or Hex-II. For clarity, Hex-I and Hex-II are colored red and blue, respectively. (A) STM image of 2D tiling composed of regular Hex-I and corresponding molecular model. (B) STM image of 2D semi-regular tiling composed of Hex-I and corresponding molecular model. The black dashed lines mark the X_4-type Br···Br interactions. (C) STM image of 2D tiling composed of Hex-II and corresponding molecular model. Imaging parameters: (A) $V_b = 300$ mV, $I_t = 800$ pA; (B) $V_b = 500$ mV, $I_t = 86$ pA; (C) $V_b = 380$ mV, $I_t = 100$ pA. All scale bars are 2 nm.

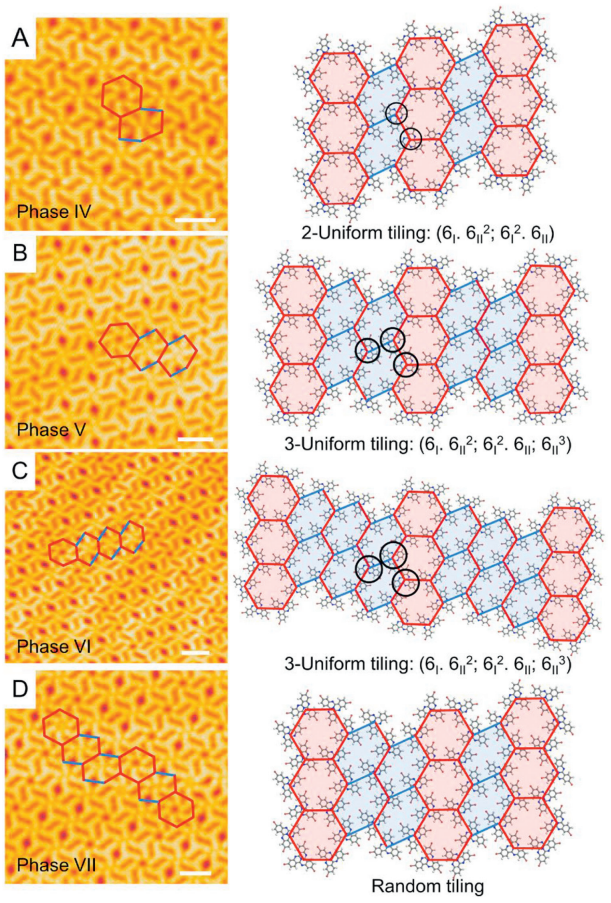

Fig. 3. 2D tessellations based on Hex-I and Hex II tiles. (A-C) STM images and corresponding molecular models for the higher-order interweaving of Hex-I and Hex-II with different composition ratios. (A) 1:1, (B) 1:2, (C) 1:3. (D) STM image and corresponding molecular model of 2D random tiling based on Hex-I and Hex-II. Imaging parameters: (A) $V_b = 260$ mV, $I_t = 80$ pA; (B) $V_b = 420$ mV, $I_t = 100$ pA; (C) $V_b = 380$ mV, $I_t = 100$ pA; (D) $V_b = 310$ mV, $I_t = 300$ pA. All scale bars are 2 nm.

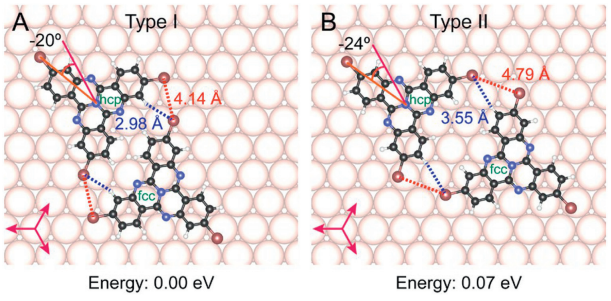

Fig. 4. DFT-optimized adsorption configurations of Type I (A) and Type II (B) dimers. The energies are relative to the Type I dimer. High-symmetry directions of the Au (111) surface are indicated at the lower left with red arrows.

bility for the Type I dimer. The DFT-optimized configurations of Type I and Type II dimers are shown in Fig. 4. In Type I dimers, the molecules are adsorbed at the hcp and fcc sites with an orientation deviating by −20° from the ⟨110⟩ direction of the substrate. In Type II dimers, the molecules also adsorbed at the hcp and fcc sites, with an orientation of −24° from the ⟨110⟩ direction of the substrate. However, the intermolecular distance varies between Type I and Type II dimers, influencing the Br-mediated interactions and consequently the stability of the dimers.

Given that the Type I dimer predominates in Hex-I and Hex-II, it can be deduced that these hexagonal tiles exhibit relatively high stability, enabling their existence on the surface to form extensive, organized molecular domains that intertwine in diverse patterns. Conversely, the prevalence of Type II dimers in Hex-III, Hex-IV, and Hex-V suggests a comparatively lower stability when compared to Hex-I and Hex-II. Consequently, Hex-III, Hex-IV, and Hex-V are unable to form 2D tessellations on the surface due to the low stability.

In conclusion, we present the regular, semi-regular and complex *k*-uniform tiling proceeded in the 2D supramolecular self-assembly of a single molecule TBTCQ. The various tessellations are built from versatile hexagonal tiles constituted of enantiopure TBTCQ dimers. Molecular modeling illustrates that the tessellations of self-assembled TBTCQ on Au (111) surface are under control of Br···Br/H contacts. Increased complexity in the self-assembled structure of TBTCQ is achieved through the variability of halogen-mediated interactions, which allows for the 2D tiling of flexible hexagonal tiles. The intricate tessellations observed in our research provide exquisite insights for understanding crystallization at the molecular scale.

Declaration of competing interest

The authors declare that they have no known competing financial interests or personal relationships that could have appeared to influence the work reported in this paper.

CRediT authorship contribution statement

Junjie Duan: Visualization, Validation, Data curation. **Dan Chen:** Resources. **Long Chen:** Resources. **Shuying Li:** Writing – original draft, Visualization. **Ting Chen:** Writing – review & edit-

ing, Project administration, Funding acquisition, Conceptualization. **Dong Wang:** Writing – review & editing, Project administration, Funding acquisition.

Acknowledgments

This work is supported by the Strategic Priority Research Program of CAS (No. XDB0520201), the National Natural Science Foundation of China ((Nos. 22132007, 22372175, 22202208, 22372030), and CAS Project for Young Scientists in Basic Research (No. YSBR-053). The Supercomputing Environment of the Chinese Academy of Sciences is acknowledged for providing computational re-sources.

Supplementary materials

Supplementary material associated with this article can be found, in the online version, at doi:10.1016/j.cclet.2024.110445.

References

[1] C.R. Pfeiffer, N. Pearce, N.R. Champness, Chem. Commun. 53 (2017) 11528–11539.
[2] M.O. Blunt, J.C. Russell, M.D.C. Giménez-López, et al., Science 322 (2008) 1077–1081.
[3] M. Pivetta, M.C. Blüm, F. Patthey, W.D. Schneider, Angew. Chem. Int. Ed. 47 (2008) 1076–1079.
[4] W. Hu, M.A. Kher-Elden, H. Zhang, et al., Nanoscale 14 (2022) 7039–7048.
[5] G. Copie, F. Cleri, Y. Makoudi, et al., Phys. Rev. Lett. 114 (2015) 066101.
[6] K. Aissou, W. Kwon, M. Mumtaz, et al., ACS Nano 10 (2016) 4055–4061.
[7] J.I. Urgel, D. Écija, G. Lyu, et al., Nat. Chem. 8 (2016) 657–662.
[8] D. Peyrot, F. Silly, Int. J. Mol. Sci. 24 (2023) 11291.
[9] L. Voigt, M. Kubus, K.S. Pedersen, Nat. Commun. 11 (2020) 4705.
[10] R. Hellwig, T. Paintner, Z. Chen, et al., ACS Nano 11 (2017) 1347–1359.
[11] J.I. Urgel, D. Ecija, W. Auwärter, et al., J. Phys. Chem. C 118 (2014) 12908–12915.
[12] S. Sun, B. Li, W. Xiong, et al., Appl. Surf. Sci. 636 (2023) 157769.
[13] L. Kormoš, P. Procházka, A.O. Makoveev, J. Čechal, Nat. Commun. 11 (2020) 1856.
[14] F. Cheng, X.-J. Wu, Z. Hu, et al., Nat. Commun. 9 (2018) 4871.
[15] J. Wang, Y. Zheng, X. Nie, et al., J. Phys. Chem. Lett. 12 (2021) 8151–8156.
[16] J. Shang, Y. Wang, M. Chen, et al., Nat. Chem. 7 (2015) 389–393.
[17] Y. Zheng, J. Wang, K. Niu, et al., J. Phys. Chem. C 126 (2022) 12009–12014.
[18] C. Deng, J. Wang, H. Zhu, et al., J. Phys. Chem. Lett. 14 (2023) 9584–9589.
[19] L. Cai, Y. Huang, D. Wang, W. Zhang, Z. Wang, A.T.S. Wee, J. Phys. Chem. Lett. 13 (2022) 2180–2186.
[20] X. Li, Z. Xu, D. Bu, et al., Chin. Chem. Lett. 36 (2025) 110100.
[21] L. Feng, T. Wang, Z. Tao, et al., ACS Nano 13 (2019) 10603–10611.
[22] Y.Q. Zhang, M. Paszkiewicz, P. Du, et al., Nat. Chem. 10 (2018) 296–304.
[23] A. Stannard, J.C. Russell, M.O. Blunt, et al., Nat. Chem. 4 (2012) 112–117.
[24] Z.Y. Yi, X.Q. Yang, J.J. Duan, et al., Nat. Commun. 13 (2022) 5850.
[25] J. Hou, B. Tu, Q. Zeng, C. Zhan, J. Yao, Chin. Chem. Lett. 31 (2020) 353–356.
[26] J. Teyssandier, K.S. Mali, S. De Feyter, ChemistryOpen 9 (2020) 225–241.
[27] B. Grünbaum, G.C. Shephard, Tilings and Patterns, W. H. Freeman, New York, 1986.